Cancer Research

CSTF2-Induced Shortening of the *RAC1* 3′UTR Promotes the Pathogenesis of Urothelial Carcinoma of the Bladder

Xin Chen[1,2], Jia-Xing Zhang[1,3], Jun-Hang Luo[4], Song Wu[5], Gang-Jun Yuan[1,2], Ning-Fang Ma[6], Yong Feng[7], Mu-Yan Cai[1], Ri-Xin Chen[1], Jun Lu[4], Li-Juan Jiang[1,2], Jie-Wei Chen[1], Xiao-Han Jin[1], Hai-Liang Liu[8], Wei Chen[4], Xin-Yuan Guan[1,9], Tie-Bang Kang[1], Fang-Jian Zhou[1,2], and Dan Xie[1]

Abstract

Shortening of the 3′ untranslated regions (3′UTR) of mRNA is an important mechanism for oncogene activation. However, 3′UTR alteration events, their pathologic functions, and underlying mechanisms in human urothelial carcinoma of the bladder (UCB) are not clear. Here, we combine RNA sequencing, bioinformatics, and clinical studies in two independent cohorts of patients with UCB to identify a novel *RAC1* shorter 3′UTR isoform that is frequently expressed in UCB and is critical in the tumorigenesis and acquisition of a poor prognostic phenotype in patients. Short 3′UTR isoform of *RAC1* substantially upregulated RAC1 expression by escaping from miRNA-targeted repression and played an essential oncogenic role in UCB pathogenesis. An important cleavage/polyadenylation factor, cleavage stimulation factor 2 (CSTF2), induced 3′UTR shortening of *RAC1* in UCB by mediating slow transcriptional elongation at *RAC1*. Cotranscriptional recruitment of CSTF2 on the GUAAU motif at proximal polyadenylation site of *RAC1* attenuated the recruitment of two transcription factors AFF1 and AFF4, causing the defects in elongation. CSTF2 regulated the tumorigenic functions of the shorter *RAC1* isoform in UCB cells, enhancing cell proliferation, migration, and invasion. The combination of high expression of CSTF2 and high usage of *RAC1* short-3′UTR isoform may be used as a powerful biomarker to predict poor prognosis in UCB. Our findings also suggest a CSTF2-regulated *RAC1*-3′UTR shortening program as an exploitable therapeutic strategy for patients with UCB.

Significance: These findings demonstrate that the short isoform of *RAC1* is critical in UCB tumorigenesis and may have implications for developing new therapeutic strategies to treat this disease. *Cancer Res; 78(20); 5848–62. ©2018 AACR.*

Introduction

Bladder cancer is one of the common cancers in the world. Urothelial carcinoma of the bladder (UCB) is the predominant histopathologic form, accounting for 90% of all diagnosed cases of bladder cancer (1). Despite advancements in surgical treatments and the development of novel drugs, approximately 50% of patients with UCB develop metastatic/recurrent disease within 2 years of diagnosis (2). Thus, understanding the molecular mechanism(s) that govern tumorigenesis and disease progression of UCB is essential to develop better treatment strategies.

It is well established that oncogene activation plays a critical role in the pathogenesis of human cancers. Recently, shortening of mRNAs' 3′ untranslated regions (3′UTR) has been reported as an important mechanism for the upregulation and/or activation of oncogene, essentially leading to the development and progression of certain malignancies (3, 4). In multiple human cancer cell lines and tissues, the 3′UTR shortening of some proto-oncogenes, in which DNA lesions are not found, is resulted from alternative cleavage and polyadenylation (APA; ref. 5). It has been reported that oncogenes favor the utilization of proximal polyadenylation sites (pPAS) located within the terminal exon proximally downstream of the stop codon (6). Thus, although the protein-coding sequence is unchanged, the regulatory elements in the 3′UTR that might impair gene's mRNA stability and/or translation efficiency can be excluded, such as miRNA-binding sites (7). In human breast, lung, colorectal, and kidney carcinomas, tumors expressing mRNAs with shorter-3′UTRs tend to be more aggressive and cause poorer patient prognosis (5, 8, 9). To date, however, 3′UTR alteration events, as well as their pathologic functions and underling mechanisms in UCB, have not been elucidated.

[1]State Key Laboratory of Oncology in South China, Collaborative Innovation Center for Cancer Medicine, Sun Yat-sen University Cancer Center, Guangzhou, China. [2]Department of Urology, Sun Yat-sen University Cancer Center, Guangzhou, China. [3]Department of Oncology, the First Affiliated Hospital, Sun Yat-Sen University, Guangzhou, China. [4]Department of Urology, the First Affiliated Hospital, Sun Yat-sen University, Guangzhou, China. [5]The Affiliated Luohu Hospital of Shenzhen University, Shenzhen Luohu Hospital Group, Shenzhen, China. [6]Key Laboratory of Protein Modification and Degradation, School of Basic Medical Sciences, Affiliated Cancer Hospital and Institute of Guangzhou Medical University, Guangzhou, China. [7]School of Basic Medical Sciences, Wuhan University, Wuhan, China. [8]CapitalBio Genomics Co., Ltd, Dongguan, Guangdong, China. [9]Department of Clinical Oncology, Li Ka Shing Faculty of Medicine, The University of Hong Kong, Hong Kong, China.

Note: Supplementary data for this article are available at Cancer Research Online (http://cancerres.aacrjournals.org/).

X. Chen, J.-X. Zhang, J.-H. Luo, S. Wu, and G.-J. Yuan contributed equally to this article.

Corresponding Authors: Dan Xie, Sun Yat-sen University Cancer Center, No. 651, Dongfeng Road East, Guangzhou, Guangdong 510060, China. Phone: 86-20-87343193; Fax: 86-20-87343170; E-mail: xiedan@sysucc.org.cn; and Fang-Jian Zhou, zhoufj@sysucc.org.cn

doi: 10.1158/0008-5472.CAN-18-0822

Herein, by deep RNA sequencing (RNA-seq) analysis, combined with two large cohorts of clinical UCB studies, we identify a novel short-3′UTR isoform of *RAC1*, generated from APA, plays an essential oncogenic role in UCB pathogenesis. Functional and mechanistic studies reveal, for the first time, that cleavage stimulation factor 2 (CSTF2) interacts with GUKKU motif downstream of *RAC1* pPAS to induce *RAC1* 3′UTR shortening in UCB cells, by slowing AFF1- and AFF4-mediated transcription elongation. Importantly, our results demonstrate that CSTF2 contributes to the tumorigenic functions of the shorter *RAC1* isoform. UCB with high expressions of both CSTF2 and shorter *RAC1* isoform exhibits a more aggressive disease and worse outcome. Our data, collectively, reveal a new cause of UCB malignancy–CSTF2-induced short-3′UTR *RAC1* isoform, and imply potentially therapeutic target for UCB.

Materials and Methods

Patients and tissue specimens

For RNA-seq, 15 cases of UCB and matched adjacent normal bladder tissues were obtained from individuals diagnosed with UCB and received radial cystectomy at Sun Yat-Sen University Cancer Center (SYSU-CC, Guangzhou, China) in 2011. For qRT-PCR and IHC analysis, UCBs with matched normal tissues were derived from 80 and 94 patients with UCB who had received radial cystectomy at SYSU-CC and the First Affiliated Hospital of Sun Yat-Sen University (SYSU-FAH), from 2005 to 2012 and from 2004 to 2012, respectively. Each subject was properly informed before recruitment for the study. Clinical information of the patients with UCB is summarized in Table 1. In addition, a panel of colorectal carcinoma, hepatocellular carcinoma, and non–small cell lung cancer with matched normal tissues (30 patients, respectively) were obtained from SYSU-CC. All specimens were snap frozen in liquid nitrogen upon collection. The tumor grade and stage were defined according to the criteria of the World Health Organization and the sixth edition of the tumor–node–metastasis classification of the International Union Against Cancer (UICC, 2009; ref. 10). All patients were followed up on regular basis, and disease-free survival (DFS) time was determined from the date of surgery to the date of the first clinical evidence of cancer recurrence and was censored at the date of death from other causes or the date of the last follow-up visit for survivors. The study was performed in accordance with the Declaration of Helsinki. Written informed consent was obtained from all the patients before the study began. This study was approved by the Institute Research Ethics Committee at Sun Yat-Sen University Cancer Center.

Total RNA extraction and RNA-seq

RNAs from tumor/normal paired UCB tissues were used to generate mRNA sequencing libraries using the TruSeq RNA sample preparation Kit (IIIumina). RNA-seq libraries were then sequenced on the HiSeq 2000 platform according to the manufacturer's recommendations. Paired-end RNA-seq reads with 90 bp in each end were aligned to the human genome (hg19) using TopHat 2.0.10 (11).

qRT-PCR and calculation of distal polyadenylation site usage

Total RNA was extracted using TRIzol reagent (Life Technologies). For qRT-PCR, the mRNA was reverse transcribed using MMLV-RT (Invitrogen) using the manufacturer's protocol to generate cDNA. The qRT-PCR reactions were performed using SYBR-GREEN (Biorad). Data were calculated using a modified version of the $2^{-\Delta\Delta C_t}$ method to show changes in distal polyadenylation site (dPAS) usage, where C_t is the threshold cycle (12). The following was calculated using primer sets designed in the common part of the isoforms of a transcript (called "common primer set") as well as in the distal part of long isoform of the same transcripts (called "distal primer set"): ΔC_t (common and distal) was normalized to the levels of 7SK, where ΔC_t (common or distal) = C_t common or distal − C_t 7SK. $\Delta\Delta C_t = \Delta C_t$ distal − ΔC_t common. To show fold changes normalized to the control siRNA-transfected samples, the following equation was used: normalized $\Delta\Delta\Delta C_t = \Delta\Delta C_t$ target siRNA − $\Delta\Delta C_t$ control siRNA. Then the increase or decrease in dPAS usage was calculated as $\pm 2^{-\text{normalized } \Delta\Delta\Delta C_t}$. Categories of high and low usage of *RAC1* with short-3′UTR in UCB

Table 1. Correlation between the usage of *RAC1* short-3′UTR and clinicopathologic characteristics of patients with UCB

	SYSU-CC cohort					SYSU-FAH cohort				
Characteristics	**Number**	**Low usage**	**High usage**	χ^2	***P* value**	**Number**	**Low usage**	**High usage**	χ^2	***P* value**
Age				0.094	0.759				1.37	0.242
>60	33	18	15			41	19	22		
<60	47	24	23			53	31	22		
Gender				3.394	0.065				1.247	0.264
Female	7	6	1			15	6	9		
Male	73	36	37			79	44	35		
T status				13.06	<0.001				6.635	0.01
T1+2	52	35	17			27	20	7		
T3+4	28	7	21			67	30	37		
N status				15.96	<0.001				7.471	0.006
N0	62	40	22			70	43	27		
N1+2	18	2	16			24	7	17		
Tumor size				28.7	<0.001				4.39	0.036
>5 cm	42	34	8			49	21	28		
<5 cm	38	8	30			45	29	16		
Grade				2.265	0.132				0.219	0.64
G1+2	49	29	20			43	24	19		
G3	31	13	18			51	26	25		
Tumor multiplicity				0.08	0.778				2.52	0.112
Unifocal	35	19	16			41	18	23		
Multifocal	45	23	22			53	32	21		

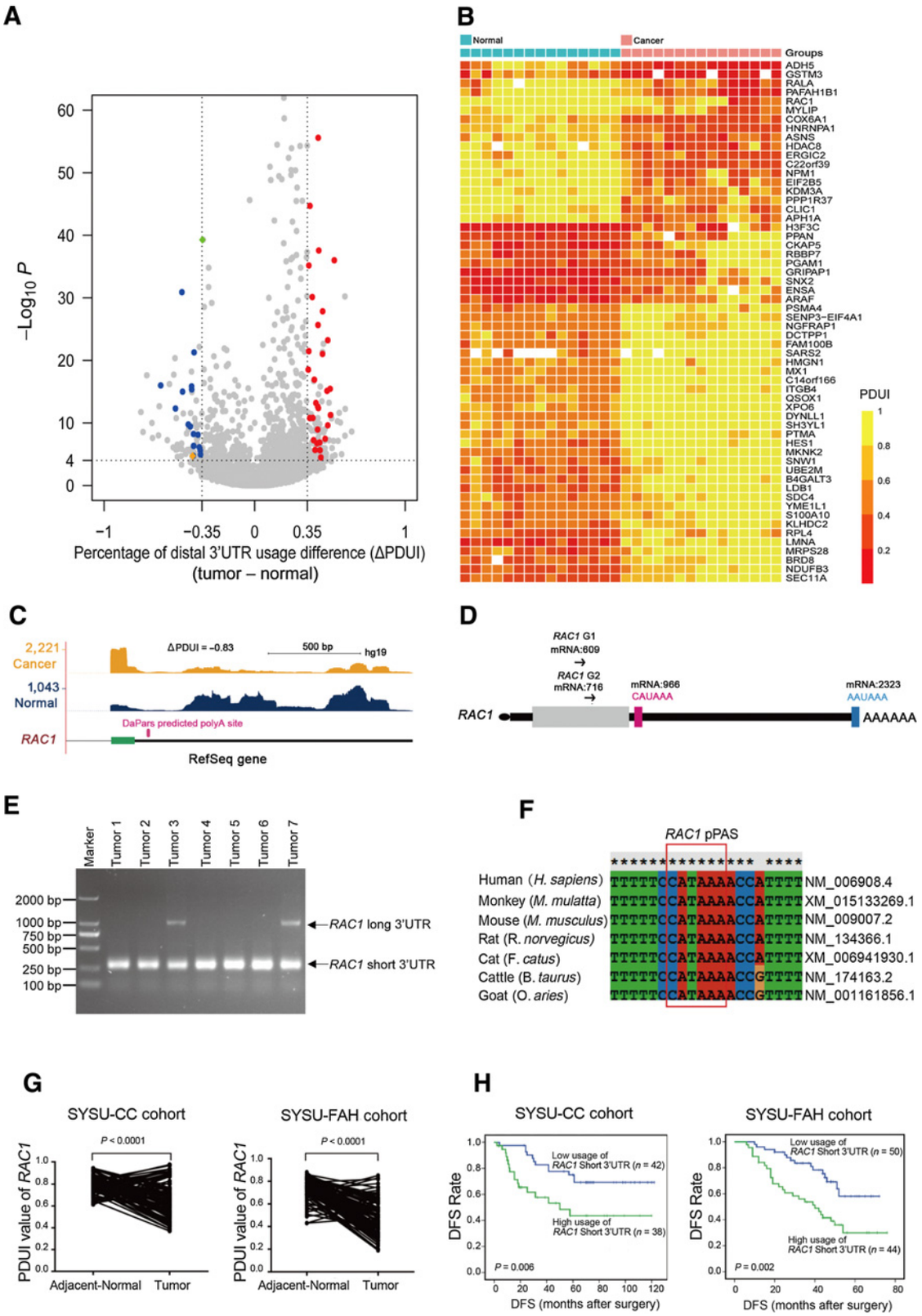

samples were defined as groups with ΔPDUII value above or below/equal to the median index.

IHC

IHC studies were performed following a standard streptavidin–biotin–peroxidase complex method (13). Slides were incubated respectively with primary antibodies against RAC1 (Proteintech), CSTF2, FIP1, CPSF6 (Abcam; 1:200 dilution), PABPN1, CFIM25 (Abcam), and CFIM68 (Santa Cruz Biotechnology; 1:500 dilution). Immunostaining was performed using the Envision System with diaminobenzidine (Dako). A negative control was obtained by replacing the primary antibody with a normal IgG. Known immunostaining-positive cases were used as positive controls.

Positive expression of RAC1 in UCB was in the cytoplasm, whereas positive expression of CSTF2, PABPN1, FIP1, CPSF6, CFIM25, and CFIM68 was in the nucleus. For evaluation of IHC staining, a previously validated semiquantitative scoring criterion was used, in which both staining intensity and positive areas were recorded (14). A staining index (values 0–9), obtained as the intensity of RAC1 or CSTF2, PABPN1, FIP1, CPSF6, CFIM25, and CFIM68-positive staining (negative = 0, weak = 1, moderate = 2, or strong = 3 scores) and the proportion of immunopositive cells of interest (<10% = 1, 10%–50% = 2, or >50% = 3 scores), was calculated. Categories of high and low expression were defined as groups with staining index above or below/equal to the median staining index. Two independent pathologists (Dr. M.-Y. Cai and D. Xie) who were blinded to the clinicopathologic information carried out the scorings. The interobserver disagreements (approximately 6% of the total informative cases) were reviewed as second time, followed by a conclusive judgment by both pathologists.

Cell lines and cell cultures

The bladder cancer cell lines, J82, T24, and 5637, and a nontumorous bladder cell line, SV-HUC-1, were purchased from the ATCC in 2013. The BIU cell line was obtained from the Institute of Urology at the First Affiliated Hospital of Peking University as a gift in 2012. J82 was cultured in DMEM (Invitrogen) supplemented with 10% FBS (HyClone). The other four lines were cultured in RPMI-1640 (Invitrogen) supplemented with 10% FBS (HyClone). All cell lines used in this study were authenticated 3 months before the beginning of the study (2014) based on viability, recovery, growth, and morphology by the supplier, and all the cell lines have not been in culture for greater than 2 months (15).

Oncogenic assays

For cell growth assay, cells were seeded in 96-well plates at a density of 1×10^3 cells per well, and cell growth rate was assessed with the CCK8 Kit (Dojindo Laboratories). For foci formation assay, 2×10^2 cells were seeded in 6-well plates, and after 2 weeks of culture, cell colonies were counted by crystal violet staining. The results are expressed as the mean ± SD of three independent experiments.

Wound-healing and invasion assays

For the wound-healing assay, UCB cells were cultured on a 6-well plate until confluence and then wounded with a 200 μL pipette tip. Migration photos were captured at 0 and 24 hours after scratching. Transwell assays using Boyden chambers containing 24-well Transwell plates (BD Inc.) with 8 mm pore size were used to evaluate the migration and invasiveness of cells. All experiments were performed in duplicate and repeated 3 times. For the invasion assay, the cell culture inserts were seeded with 5×10^4 cells in 500 μL of serum-free medium without an extracellular matrix coating. 1640 medium containing 20% FBS was added to the bottom chamber. After approximately 24 hours of incubation, the cells on the lower surface of the filter were fixed, stained, and examined using a microscope.

Animal experiments

All procedures involving mouse were approved by the Institutional Animal Care and Use of SYSU-CC. All mice were obtained from Charles River Laboratories. Xenograft tumor growth assay was established by subcutaneous injection of 1×10^6 UCB cells into the right dorsal flank of 4-week-old Balb/c nude mice. Tumor formation in the mice was checked after 4 weeks. *In vivo* metastasis model was established by i.v. injection of 2×10^5 UCB cells through tail vein into each 4-week-old Balb/c nude mice. Six weeks after injection, the mice were sacrificed. The lungs were removed and fixed with phosphate-buffered formalin. Subsequently, consecutive tissue sections were made for each block of the lung. The numbers of pulmonary metastatic nodules in the lung were carefully examined. For imaging tumors in live animals, VivoGloluciferin (Promega) was dissolved in sterilized PBS (finally 40mg/mL). Mice were anaesthetized with isoflurane and injected intraperitoneally with 100 μL of the luciferin solution. After 5 minutes, images were acquired with the Xenogen IVIS Lumina series II and analyzed using the LivingImage 2.11 software package (Xenogen Corp.).

Figure 1.

3′UTR shortening of *RAC1* identified by DaPars analysis on RNA-seq. **A,** Fifty-eight significant and reproducible 3′UTR alteration events were identified by DaPars from RNA-seq on 15 UCB and paired adjacent normal bladder tissues. Volcano plot compares ΔPDUI values for UCB tissues versus adjacent normal bladder tissues. Positive values on the *x*-axis indicate 3′UTR lengthening in tumor tissue, whereas negative values indicate 3′UTR shortening events. The statistical significance ($-\log_{10}P$) is shown on the *y*-axis. Red dots and blue dots represent genes with significant 3′UTR lengthening or shortening in UCB tissues, respectively. The green dot represents the ΔPDUI value of *RAC1*, whereas the orange dot represents the ΔPDUI value of *RALA*. **B,** Heat map showing the PDUI value of 58 significant and reproducible 3′UTR alterations in genes from 15 UCB tissues (pink group) and matched adjacent normal tissues (blue group). **C,** Representative RNA-seq density plots along with ΔPDUI values for *RAC1* in a UCB tissue (orange plot) and matched normal tissue (blue plot). Numbers on the *y*-axis indicate RNA-seq read coverage. Schematic representation of the pPAS in *RAC1* is shown in the bottom plot. Black, UTR region; green, the protein-coding region (CDS) of *RAC1*; pink, novel PAS of *RAC1*. **D,** Primer sequences used in 3′RACE are indicated on the schematic above the graphs. Gray box, CDS; black box, UTR. The pink box and CAUAAA represent the pPAS identified by 3′RACE; the blue box and AAUAAA represent the dPAS. **E,** Agarose gel electrophoresis demonstrates 3′RACE amplification of *RAC1* using RNAs extracted from seven UCB tissues as templates. Lane 1, marker; lanes 2–8, 3′RACE *RAC1* fragment amplified from seven UCB tissues with G2 and inner primers. **F,** DNA sequence alignment of the pPAS region of *RAC1* from seven different mammalian species using MEGA6 software. The pPAS of *RAC1* is indicated by the red frame. **G,** A scatter plot illustrating qRT-PCR analysis of PDUI value for *RAC1* in UCB tissues compared with matched adjacent normal bladder tissues from the SYSU-CC (left) and SYSU-FAH (right) cohorts. $P < 0.001$, paired Student *t* test. **H,** Kaplan–Meier curves with univariate analyses of DFS ($P < 0.01$, log-rank analysis) in patients with UCB with low versus high usage of the *RAC1* short 3′UTR from SYSU-CC (left) and SYSU-FAH (right) cohorts.

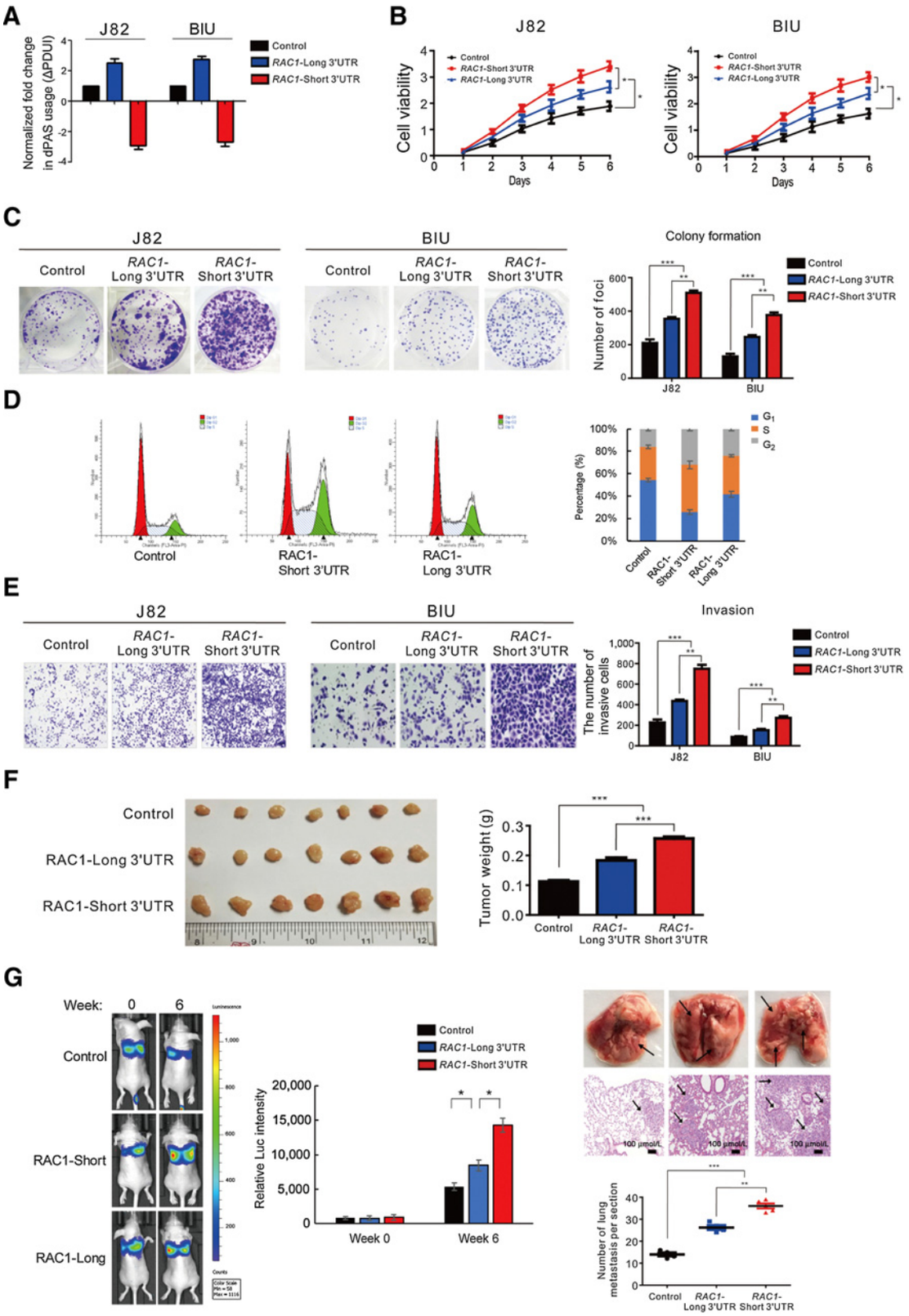

5,6-Dichlorobenzimidazole 1-β-D-ribofuranoside transcription elongation assay

The labeling of nascent RNA with bromouridine (BrU) was carried out as previously described (16, 17). The drug 5,6-dichlorobenzimidazole 1-β-D-ribofuranoside (DRB; Sigma) is added to the media to a final concentration of 100 μmol/L, and cells are incubated for 3 hours at 37°C. After the incubation with DRB, the cells were washed with PBS twice, and nascent RNA was labeled in conditioned media containing 2 mmol/L BrU (Sigma) for indicated time points at 37°C. The cells were then directly lysed in TRIzol reagent (Invitrogen). Total RNA was isolated, and the Bru-labeled RNA was isolated from the total RNA by incubation with anti-BrdUrd antibodies conjugated to agarose Dynabeads (Santa Cruz Biotechnology) under gentle rotation for 1 hour at 4°C. Finally, purified RNA was reverse transcribed. Oligonucleotides (5′-3′) used for qRT-PCR are listed below:

RAC1 Exon1–Intron1 (Forward): ATGCAGGCCATCAAGTGTGT
RAC1 Exon1–Intron1 (Reverse): GGAGTTCACTTTTCCCTCTAGC
RAC1 Intron6–Exon7 (Forward): CTGTGGGTCTTAACGTCAGC
RAC1 Intron6–Exon7 (Reverse): TCGCTTCGTCAAACACTGTC

Statistical analyses

Statistical analysis in SYSU-CC and SYSU-FAH cohorts was carried out with SPSS software (SPSS Standard version 13.0; SPSS Inc. Chicago). The χ^2 test was used to assess the statistical significance of the association of the expression of *RAC1* and *RALA* with short-3′UTR or CSTF2 with the patient's clinicopathologic parameters and its correlation. Comparisons between groups for statistical significance were performed with the independent sample *t* test. DFS was assessed with the Kaplan–Meier method and compared by the log-rank test. Correlations were analyzed by the Pearson correlation test. *P* values of < 0.05 were considered significant.

For survival analysis in The Cancer Genome Atlas (TCGA) cohorts, we used the X-tile software version 3.6.1 (18) built-in validated feature that automatically defined the optimal cut-off point. Data were downloaded from Firehose (http://gdac.broadinstitute.org). R software version 3.3.1 (R Foundation for Statistical Computing) and OriginPro 9 (OriginLab) were used for performing statistical tests and plotting.

Data and software availability

RNA-seq data are accessible using Biosample ID: AMN06112418-SAMN06112447.

Supplementary information

Supplementary Information includes Supplementary Materials and Methods, four Supplementary Figures, and four Supplementary Tables.

Results

Short-3′UTR isoform of *RAC1* is predominantly expressed in human UCBs and is associated with patients' advanced clinical stage and poor outcome

In this study, we first performed deep RNA-seq in 15 pairs of UCB and adjacent normal bladder tissues with a bioinformatics algorithm, Dynamic Analysis of Alternative Polyadenylation from RNA-Seq (DaPars; ref. 12), to characterize significant 3′UTR alteration events. When applied to the 25,293 Refseq transcripts, 58 statistically significant and reproducible 3′UTR alteration events were identified, including 40 genes with 3′UTR lengthening and 18 genes with 3′UTR shortening in UCB tissues compared with matched normal tissues (Fig. 1A; Supplementary Table S1). We next applied KEGG analysis to identify APA genes that play critical roles in cancer-related pathway. The results showed that the *RAC1* and the *RALA*, two critical genes in Ras-related cancer signaling (19, 20), were predominantly expressed with shortened 3′UTR in UCB tissues, respectively (Fig. 1B and C; Supplementary Fig. S1A; Supplementary Table S2).

To investigate if the observed 3′UTR shortening of *RAC1* and *RALA* is due to utilization of novel pPAS signals within these two genes, 3′ rapid amplification of cDNA ends (3′RACE) was performed in 7 UCB tissues using primers described in Fig. 1D and Supplementary Fig. S1B. The authenticity of novel pPAS in *RAC1* and *RALA* was discovered within our tested tissues, respectively. For the shorter mRNA isoforms of *RAC1*, a weak pPAS CAUAAA was used (Fig. 1E), and a canonical PAS AAUAAA was confirmed for the shorter mRNA isoforms of *RALA* (Supplementary Fig. S1C). The two pPAS signals in *RAC1* and *RALA* are conserved at the orthologous position in six mammal species (Fig. 1F; Supplementary Fig. S1D).

To study the clinical significance of *RAC1* and *RALA* short-3′UTR isoforms expression in patients with UCB, two independent UCB cohorts were recruited from the SYSU-CC and SYSU-FAH, in which 80 and 94 pairs of UCB and matched normal bladder tissue samples were collected, respectively. The degree of difference of 3′UTR usage of *RAC1* and *RALA* between the samples was quantified as a change in percentage dPAS usage index (ΔPDUI), which can identify lengthening (positive index) or shortening (negative index) within the 3′UTR. The PDUI value was significantly decreased in UCB tissues compared with

Figure 2.

The *RAC1* short-3′UTR isoform has oncogenic functions and increases aggressiveness in UCB cells. **A,** qRT-PCR results shown as fold change in dPAS usage (ΔPDUI) in UCB cell lines transfected with the *RAC1* short- or long-3′UTR isoform compared with cells transfected with control vector. All graphs represent the mean ± SD of at least three independent experiments. **B–D,** Ectopic overexpression of the *RAC1* short-3′UTR isoform in UCB cell lines significantly increases cell growth (**B**), colony formation (**C**), and S phase (**D**), as compared with overexpression of the *RAC1* isoform with long 3′UTR or transfection of control vector, as measured by CCK-8, colony formation, and flow cytometry, respectively. All graphs represent the mean ± SD obtained from three independent experiments. *, $P < 0.05$; **, $P < 0.01$, Student *t* test. **E,** Transwell assay analyses of the migration ability of the indicated UCB cells. **F**, Ectopic overexpression of the *RAC1* short-3′UTR isoform in the UCB BIU-87 line substantially promoted tumor formation compared with overexpression of *RAC1* with long 3′UTR or transfection with control vector. Left, images of the xenograft tumors formed in Balb/c nude mice injected with BIU-87 cells expressing *RAC1* short- or long-3′UTR isoforms, or control vector. Weights of xenograft tumors are summarized in the right panel. **G,** BIU-87 cells infected with the indicated lentiviruses for the indicated *RAC1* isoforms were injected into the vein of Balb/c nude mice, followed by noninvasive bioluminescence imaging for 6 weeks. Representative bioluminescent imaging (left), representative images of lungs (top right), and metastatic nodules (arrows) are shown. Middle, mean bioluminescent signals ($n = 5$). Bottom left, hematoxylin and eosin staining of lung metastatic lesions (original magnification, ×100; scale bar, 100 μm). The number of metastatic nodules formed in the lungs of nude mice is summarized for each group tested ($n = 5$) in the right bottom panel.

matched normal tissues ($P < 0.001$, Fig. 1G; Supplementary Fig. S1E), suggesting a high incidence of *RAC1* and *RALA* short-3′UTRs in UCBs. Further statistical analysis revealed that UCBs had higher expression of the *RAC1* short-3′UTR isoform, were positively associated with an advanced T and N status and larger tumor size, and displayed poorer disease-free survival (DFS, $P < 0.05$, Fig. 1H; Table 1). In contrast, no significant association between short-3′UTR *RALA* expression and patients' DFS was evaluated in these two UCB cohorts (Supplementary Fig. S1F). These results, taken together, suggested that the shortening of *RAC1* 3′UTR by APA is a frequent molecular event presented in UCB pathogenesis.

To determine if the shortening of *RAC1* 3′UTR was present in other types of human cancers, we further examined the usage of *RAC1* short-3′UTR in a series of other cancer types, including colorectal carcinoma, hepatocellular carcinoma, and non–small cell lung cancer (30 patients, respectively). The usage of short isoform of *RAC1* 3′UTR was significantly increased in these cancers compared with that of matched normal tissues ($P < 0.001$, Supplementary Fig. S1G). Further, 3′RACE identified the usage of pPAS in the tested tissues (Supplementary Fig. S1H). These results, taken together, suggested the shortening of *RAC1* 3′UTR by APA is a bona fide molecular event presented in many types of human cancer, including UCB.

RAC1 short-3′UTR isoform enhances UCB cells' oncogenic and metastatic capacities both *in vitro* and *in vivo*

To study the biological functions of distinct *RAC1* isoforms in UCB cells, we stably transfected short- or long-3′UTR isoforms of *RAC1* into two UCB cell lines (BIU-87 and J82), which had lower expression of the short *RAC1* isoform (Supplementary Fig. S2A). The transfection efficiency is shown in Fig. 2A. We found that enforced expression of the shorter-3′UTR isoform of *RAC1* in UCB cells dramatically increased cell growth (Fig. 2B), colony formation (Fig. 2C), and fraction of S phase cells (Fig. 2D), and enhanced cell-invasive ability (Fig. 2E), when compared with that of ectopic expression of full-length *RAC1* and vector control cells. Moreover, enforced expression of the shorter-3′UTR isoform of *RAC1* in a nontumorous cell line, SV-HUC-1, dramatically increased cell growth, colony formation, and cell-invasive ability (Supplementary Fig. S2B), when compared with that of ectopic expression of full-length *RAC1* and vector control cells.

Next, in two nude mouse models (i.e., a subcutaneous xenograft tumor mouse model and an *in vivo* tumor metastasis mouse model), we further observed that enforced expression of the shorter-3′UTR isoform of *RAC1* in UCB cells substantially enhanced the abilities of subcutaneous tumor formation (Fig. 2F) and cancer cells' metastatic capacities to the lungs (Fig. 2G) of mice, as compared with that of either ectopic expression of full-length *RAC1* or control cells.

The *RAC1* short-3′UTR isoform produces more RAC1 protein due to escaping from miRNA-targeted repression

In our study, we further observed that enforced expression of the short-3′UTR *RAC1* isoform substantially upregulated the protein expression of RAC1, as compared with transfection with the long-3′UTR *RAC1* isoform (Supplementary Fig. S2C). This observation was consistent with the enhanced luciferase activity examined from the luciferase reporter carrying *RAC1* short-3′UTR when compared with the *RAC1* long 3′UTR (Supplementary Fig. S2D), suggesting that short isoform of *RAC1* may be lacking repression motif presented in the full-length 3′UTR.

To test this hypothesis, we then mutated three miRNA-complementary sites in the wild-type full-length *RAC1* 3′UTR and inserted it downstream of a luciferase reporter gene, respectively. We found that loss of these miRNA-targeting sites led to a roughly 1.5-fold increase in luciferase activity compared with the luciferase reporter with intact miRNA sites (Supplementary Fig. S2E and S2F). These data, collectively, suggested that high levels of RAC1 protein produced by *RAC1* with short-3′UTR may, at least partially, be due to the loss of targeted repression on *RAC1* mediated by miRNAs.

In addition to enhanced RAC1 expression, ectopic overexpression of *RAC1* short-3′UTR isoform in UCB cells efficiently upregulated the AKT pathway and the β-catenin-MMP9 pathway (Supplementary Fig. S2C), which can potently stimulate cancer cells' proliferation and/or aggressiveness.

Enrichment of CSTF2 on *RAC1* GUKKU motif promotes 3′UTR shortening of *RAC1*

One of the most interesting questions that arose from our findings was what are the potential mechanisms governing 3′UTR shortening of *RAC1* in UCB? Because APA was initially found to be regulated in *cis* through genetic aberrations of DNA (4, 21), we thus searched for *RAC1* mutations in UCBs from the TCGA database. Of the four *RAC1* mutations we found in UCB tissues, all were located in the CDS of *RAC1* (Supplementary Table S3), indicating that the 3′UTR shortening of *RAC1* is probably not due to aberrations in *cis*-elements.

We then wondered if the global shortening of the *RAC1* 3′UTR in UCB is the result of aberrant expression of polyA *trans*-factors. We first examined the correlations between use of the *RAC1* short-3′UTR and expressions of six important cleavage/polyadenylation (CPA) factors, including CSTF2 (22), CPSF6 (23), CFIm25 (12), CFIm68 (24), PABPN1 (25), and FIP1 (26), in our two UCB tissue cohorts. The results evaluated that use of the *RAC1* short-3′UTR in UCBs was positively correlated with the expression levels of CSTF2 ($P < 0.001$, Fig. 3A), but not with the levels of the other five APA factors ($P > 0.05$; Supplementary Fig. S3A–S3E).

Subsequently, we knocked down these six CPA factors in T24 UCB cells (Supplementary Fig. S3F) and examined their effects on affecting the expression levels of different *RAC1* isoforms. Our results showed that the silence of CSTF2, but not that of the other 5 factors, dramatically affected the ratio of *RAC1* dPAS usage in cells (Fig. 3B). Two shRNAs were then used to efficiently suppress CSTF2 expression in 2 UCB cell lines, T24 and 5637 (Fig. 3C, left), which have higher usage of the *RAC1* short-3′UTR (Supplementary Fig. S2A). Northern blot demonstrated that the levels of *RAC1* short-3′UTR isoform were decreased in both CSTF2-silenced UCB cell lines, whereas the levels of the long isoform were increased in the same RNA extracts (Fig. 3C, right). qRT-PCR results further confirmed the increased ratio of *RAC1* dPAS usage in CSTF2-silenced cells (Supplementary Fig. S3G). These data revealed that, in the absence of CSTF2, the PAS of *RAC1* shifted from pPAS to dPAS, producing *RAC1* mRNAs with longer 3′UTRs in UCB cells, suggesting that CSTF2 is a key regulator of PAS choice in *RAC1*.

To test whether or not CSTF2 has a direct role on *RAC1* 3′UTR shortening, we performed RNA immunoprecipitation (RIP) assay to determine the association of CSTF2 on *RAC1* 3′UTR. CSTF2 was observed highly recruited to the region around *RAC1* pPAS

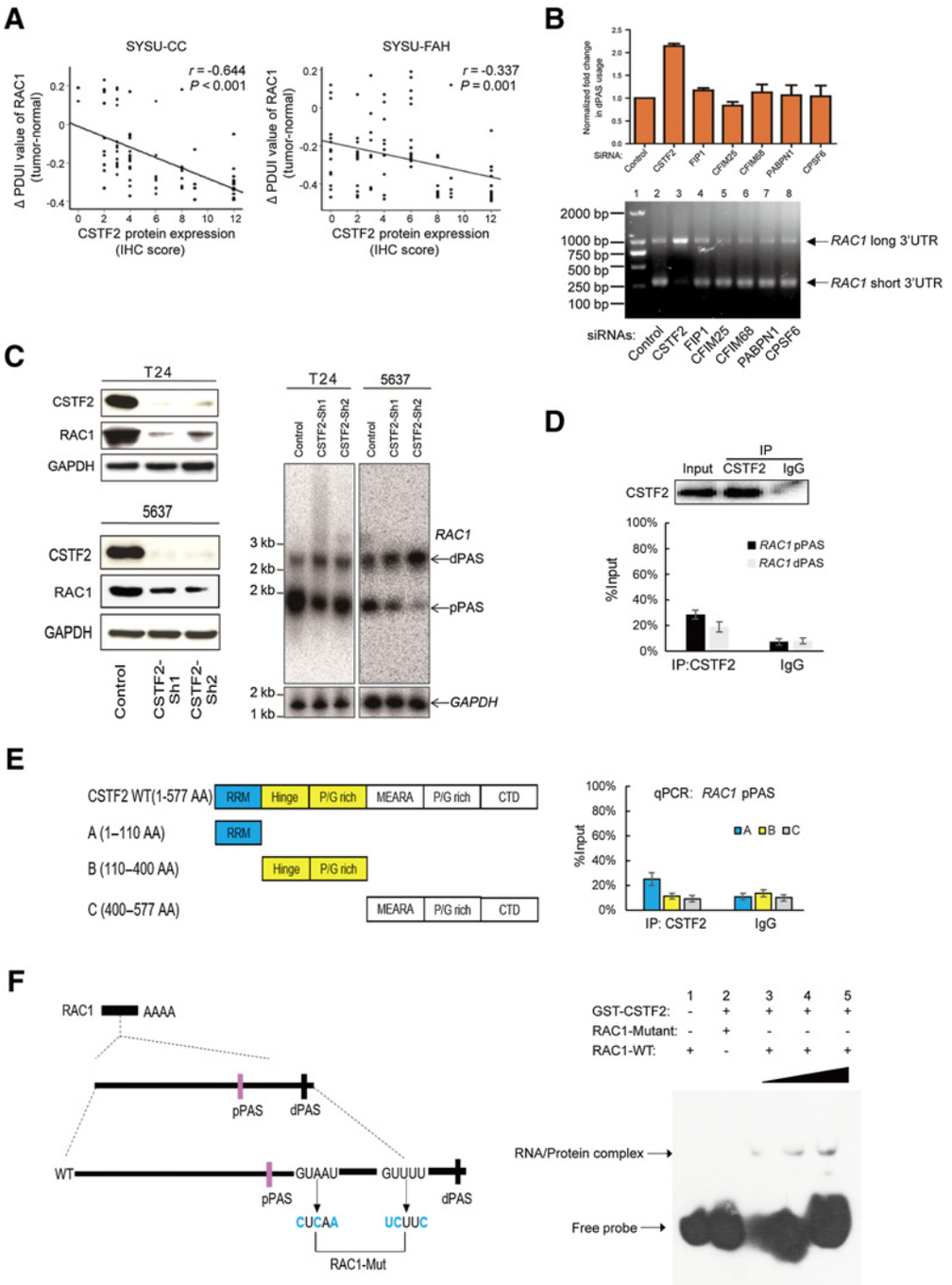

Figure 3.

CSTF2 controls PAS selection of *RAC1* in UCB. **A,** Spearman correlation analysis demonstrates that the dPAS usage of *RAC1* is negatively correlated with CSTF2 protein expression in UCB tissues from the SYSU-CC (left) and SYSU-FAH (right) cohorts. **B,** qRT-PCR result of *RAC1* is shown as fold change in dPAS usage in UCB cells after knockdown of each APA factor as indicated (top). Agarose gel electrophoresis demonstrates 3′RACE amplification of *RAC1* using RNAs extracted from UCB cells' knockdown of each indicated APA factors. Lane 1, marker; lanes 2–8, 3′RACE *RAC1* fragments amplified from UCB cells after knockdown of each indicated APA factors (bottom). **C,** Western blot analysis of CSTF2-knockdown efficiencies by two shRNAs in 5637 and T24 UCB cells. GAPDH expression was used as a loading control (left). Northern blot analysis of total polyA$^+$ RNA prepared from 5637 and T24 cells transfected with either control shRNA or two shRNAs targeting *CSTF2*. Blots were probed for *RAC1* and *GAPDH* mRNAs (right). **D,** RIP assays show association of CSTF2 with *RAC1* 3′UTR. Top, immunoprecipitation efficiency of CSTF2 antibody is shown in Western blot. Bottom, relative enrichment (mean ± SD) represents RNA levels associated with CSTF2 relative to an input control from three independent experiments. IgG antibody served as a control. **E,** Deletion mapping of the *RAC1* pPAS-binding domain in CSTF2. Left, diagrams of full-length CSTF2 and the deletion fragments. Middle, immunoprecipitation efficiency of Flag-tagged CSTF2-domain truncated mutants as shown in Western blot. Right, RIP assays show association of truncated CSTF2 with *RAC1* 3′UTR. Relative enrichment (mean ± SD) represents RNA levels associated with truncated CSTF2 relative to an input control from three independent experiments. IgG antibody served as a control. **F,** Biotin-labeled oligonucleotides containing two GUKKU motif or mutant motif from *RAC1* mRNA (left) were incubated with 50 μmol/L GST-CSTF2 protein and analyzed by EMSA assay (right).

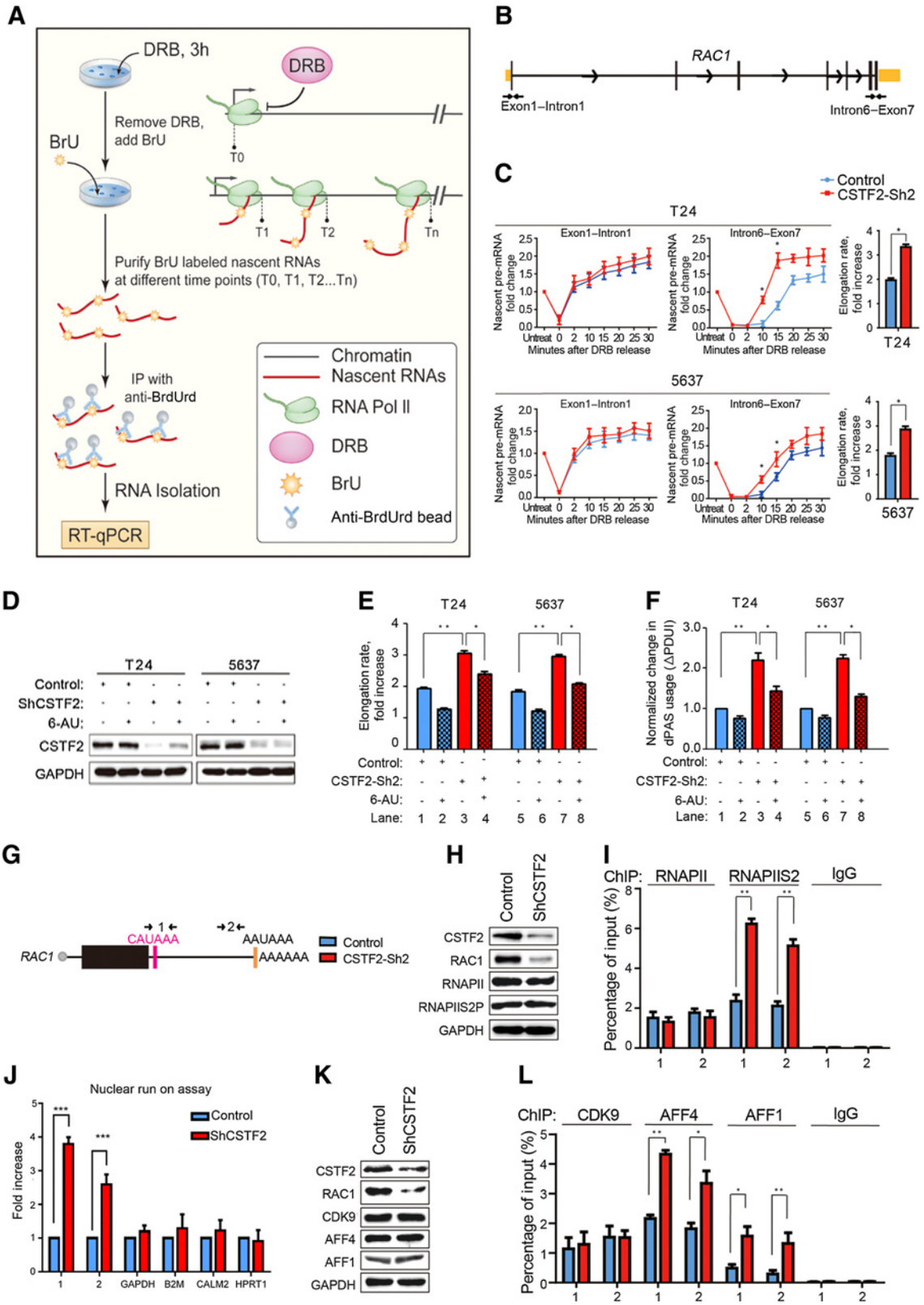

(Fig. 3D). We next mapped the domains that mediate the association of CSTF2 to *RAC1* pPAS (27). With overexpression of truncated Flag-CSTF2, we purified recombinant CSTF2–RNA complex with Flag antibody. Our RIP results showed that RNA-recognition motif domain (1–110 aa) of CSTF2 specifically interacted with *RAC1* pPAS (Fig. 3E).

We next investigated if individual motif in *RAC1* mRNA contributes to noncanonical PAS recognition by CSTF2. We examined two GUKKU motif that has been suggested to be enriched in CSTF2-sensitive noncanonical PAS (28), locating in the 30–50 nt region downstream to the noncanonical pPAS of *RAC1*. RNA electrophoretic mobility shift assay (RNA EMSA) further revealed that CSTF2 binds to *RAC1* pPAS region surrounding GUKKU motifs *in vitro* (Fig. 3F, lanes 3–5), whereas after mutation of these two motifs, the interaction of CSTF2 on *RAC1* was diminished (Fig. 3F, lane 2), indicating that GUKKU motifs downstream of *RAC1* pPAS region are critical for CSTF2 interaction.

High CSTF2 occupancy governs pPAS selection through modulation of slow RNA polymerase II transcription elongation rate at the *RAC1* locus

How does CSTF2 promote the selection of pPAS on *RAC1*? Considering that CSTF2 cotranscriptionally assembles on the carboxyl-terminal domain (CTD) of RNA polymerase II (RNAPII; ref. 29), it is very likely that CSTF2 may control PAS selection of *RAC1* by affecting RNAPII transcription kinetics. To test this hypothesis, we used DRB treatment in combination with qRT-PCR analysis to compare RNAPII elongation rates at *RAC1* in CSTF2-silenced and control UCB cells. This procedure is illustrated in Fig. 4A, in which the positions of PCR products in DRB-elongation rate analyses are shown in Fig. 4B. As anticipated, transcription in the first, promoter-proximal exon–intron junction was indistinguishable between control- and CSTF2-silenced UCB cells (Fig. 4C, left). With time progressed, we found that transcripts were observed further into the gene. *RAC1* pre-mRNA levels at the Intron 6–Exon 7 junction, which is 27 kB downstream from the transcription start site, rose markedly earlier in CSTF2-silenced cells at 10 to 15 minutes (Fig. 4C, left). This was corresponded to an overall increase in mean elongation rate across the *RAC1* gene in CSTF2-silenced cells (Fig. 4C, right). These data indicated that CSTF2 slows the transcription elongation kinetics of *RAC1*.

To validate if transcription kinetics contribute to PAS selection in *RAC1* by CSTF2, we further used 6-azauracil (6-AU), a reagent that can slow down transcription elongation (30), to treat CSTF2-silenced and control UCB cells (Fig. 4D). The results demonstrated that treatment of 6-AU could significantly prevent CSTF2-silence induced fast *RAC1* transcription rates (Fig. 4E). Furthermore, after the treatment of 6-AU, CSTF2-silence–induced usage of *RAC1* dPAS was clearly attenuated (Fig. 4F). These results provide evidence that, in UCB cells, CSTF2 deficiency can increase fast transcription rates, which in turn facilitate the utilization of dPAS on *RAC1*, whereas slowing transcription with 6-AU treatment can partially mimic the effect of CSTF2, promoting the utilization of *RAC1* pPAS.

CSTF2 attenuates the recruitment of two core super elongation complex factors, AFF1 and AFF4, to the *RAC1* pPAS, which reduces transcription elongation kinetics

To investigate the precise molecular mechanisms that speed up transcription elongation of *RAC1* after CSTF2 silencing in UCB cells, we further analyzed the effect of CSTF2 knockdown in the phosphorylation of RNAPII Serine-2 (Ser2P) at *RAC1*'s pPAS and dPAS sites (Fig. 4G), which are critical for transcription elongation. Our results showed that silence of CSTF2 did not alter the expression levels of total RNAPII and Ser2P in UCB cells (Fig. 4H) and, meanwhile, did not affect the recruitment of total RNAPII on *RAC1* 3′UTR (Fig. 4I). However, silence of CSTF2 could dramatically increase Ser2P at the pPAS region of *RAC1* (Fig. 4I). Furthermore, our Nuclear Run-On transcription assays (NRO) confirmed that RNAPII transcription in the *RAC1* pPAS region was highly increased relative to the dPAS region after CSTF2 knocking down, but such was not detected in other cellular genes, including *GAPDH*, *B2M*, *CALM2*, and *HPRT1* (Fig. 4J). These results, collectively, suggest that the deficiency of CSTF2 in UCB cells enhances Ser2P-mediated transcription elongation at *RAC1*'s pPAS.

We next wondered if the increase of Ser2P observed in CSTF2-silenced UCB cells is due to enhanced recruitment of super elongation complex (SEC), which is indispensable for Ser2P productive elongation (31). Therefore, we examined and compared the expression levels of CDK9 (the catalytic subunit in the positive elongation factor b complex, P-TEFb) and two SEC core subunits, AFF1 and AFF4 (32), as well as their enrichment status at the pPAS and dPAS regions of *RAC1*, between control and

Figure 4.

CSTF2 attenuates transcription elongation rate of *RAC1*, which contributes to pPAS selection of *RAC1*. **A,** A workflow of BrU–qRT-PCR elongation rate analysis on nascent RNA. Cells were treated with DRB for 3 hours to block transcription, and newly synthesized BrU-labeled total RNAs were collected at different time points after DRB removal. BrU-labeled nascent RNAs were then purified with anti-BrdUrd antibodies conjugated to agarose beads, followed by RNA extraction and qRT-PCR. **B,** Diagram demonstrates the positions of PCR products in DRB-elongation rate analyses. **C,** Nascent mRNA production (quantified by qRT-PCR) in different regions of *RAC1* after release from DRB inhibition in control (blue line) or CSTF2-depleted (red line) T24 or 5637 cells (left). The fold change of elongation rate was calculated for *RAC1* in control (blue bar) or CSTF2-depleted (red bar) UCB cells, and is presented in the right panel. **D,** CSTF2-knockdown efficiency was assessed by Western blot in 6-AU–treated or untreated T24 and 5637 cells. GAPDH expression was used as loading control. **E,** Elongation rate measured for *RAC1* in control (blue bar) or CSTF2-silenced (red bar) cells in the presence (lanes 2, 4, 6, and 8) or absence (lanes 1, 3, 5, and 7) of 6-AU treatment. **F,** qRT-PCR results of *RAC1* shown as fold change in dPAS usage in control (blue bar) or CSTF2-depleted (red bar) cells in the presence (lanes 2, 4, 6, and 8) or absence (lanes 1, 3, 5, and 7) of 6-AU treatment. **G,** Diagram demonstrates the positions of PCR products used for ChIP analyses. **H,** CSTF2-knockdown efficiency was assessed by Western blot. Total lysates from T24 cells were also blotted with RNAPII, RNAPII Ser2P, and RAC1 antibodies. GAPDH expression was used as loading control. **I,** ChIP assays were performed to measure the occupancy and modification of RNAPII-CTD using the indicated antibody and chromatin from control (blue bar) or CSTF2-silenced (red bar) T24 cells. Genomic DNA was amplified by the indicated primers via qPCR. Results are presented as percentage of input. **J,** NRO performed using nuclei prepared from control (blue bar) or CSTF2-depleted (red bar) T24 cells. Regions amplified by qPCR are indicated above the graph. Values were normalized to control cells. **K,** CSTF2-knockdown efficiency was assessed by Western blot, using indicated antibodies. Total lysates from T24 cells were also blotted with CDK9, AFF4, AFF1, and RAC1 antibodies. GAPDH expression was used as a loading control. **L,** ChIP assays were performed to measure the enrichments of CDK9 (the P-TEFb complex kinase) and two SEC core factors, AFF1 and AFF4, using the indicated antibody and chromatin from control (blue bar) or CSTF2-depleted (red bar) T24 cells. Genomic DNA was amplified by indicated primers from qPCR. Results are presented as a percentage of input. All graphs represent the mean ± SD obtained from at least three independent experiments. *, $P < 0.05$; **, $P < 0.01$, Student *t* test.

CSTF2-silenced UCB cells. We observed that knockdown of CSTF2 did not affect the global protein levels of CDK9, AFF4, and AFF1 in UCB cells (Fig. 4K). However, our chromatin immunoprecipitation (ChIP) assays showed that knockdown of CSTF2 did not alter the enrichment level of CDK9, but substantially increased the enrichment of both AFF4 and AFF1 on the *RAC1* pPAS region (Fig. 4L). These results, together, provide evidences that CSTF2 attenuates the recruitment of AFF4 and AFF1 to the *RAC1* pPAS region and Ser2P, resulting in a slow transcription elongation.

CSTF2 regulates the oncogenic and invasive functions of the short *RAC1* isoform in UCB cells

To investigate if CSTF2 contributes to the oncogenic and/or invasive functions of the *RAC1* short-3′UTR isoform in UCB cells, we further stably knocked down CSTF2 in two UCB cell lines, T24 and 5637, which have higher usage of the *RAC1* short-3′UTR. We observed that knockdown of CSTF2 (Fig. 5A) clearly decreased the levels of *RAC1* short-3′UTR isoform in UCB cells (Fig. 3C), and concurrently, substantially suppressed cell growth, colony formation, migration, and invasion compared with that of control cells (Fig. 5B–E; Supplementary Fig. S4A–S4C). However, enforced overexpression of the short-3′UTR isoform of *RAC1* in CSTF2-silenced UCB cells (Fig. 5A) largely prevented the decreased cell growth, colony formation, migration, and invasion by CSTF2 knocking down (Fig. 5B–E; Supplementary Fig. S4A–S4C).

Our *in vivo* mouse model studies also showed similar biological effects of CSTF2 silencing in UCB cells. The size and weight of subcutaneous xenograft tumors (Fig. 5F), as well as the lung metastatic ratio (Fig. 5G), were significantly decreased in mice injected with CSTF2-silenced UCB cells compared with that of control vector cells. Enforced expression of the short-3′UTR isoform of *RAC1* in CSTF2-silenced cells, however, substantially rescued UCB cells' potential for tumor formation and metastasis to the lung (Fig. 5F and G).

Dual high expression of CSTF2 and the short-3′UTR isoform of *RAC1* predict the worst prognosis for patients with UCB

To determine the clinical relevance of CSTF2 regulation in UCB patients, we first compared the expression of *CSTF2* mRNA in the TCGA RNA-seq data derived from 19 UCB and paired normal tissues. We discovered that the expression of *CSTF2* mRNA was significantly upregulated in UCB tissues ($P = 0.0005$, Fig. 6A). Further, the Kaplan–Meier analysis of 408 UCB tissues derived from TCGA clearly showed that high expression of *CSTF2* was significantly associated with poor patient DFS ($P = 0.0159$, Fig. 6B, log-rank test). Similar results were also obtained from our patients with UCB in either the SYSU-CC or the SYSU-FAH cohort (Fig. 6C). Furthermore, high expression of the CSTF2 protein predicted advanced tumor stage (Supplementary Table S4). Moreover, patients with UCB with both high expression of CSTF2 and high usage of the *RAC1* short-3′UTR isoform had the poorest DFS in our two cohorts (Fig. 6D).

Discussion

Human cancer is a complex disease driven by the activation of oncogenes and/or inactivation of tumor suppressors. It has been suggested that shortening of 3′UTRs is one of the important mechanisms for oncogene activation (3, 4). In UCB, however, little is known if certain oncogenes may be activated through 3′UTR shortening. In the current study, by using RNA-seq, combined with bioinformatics and clinical studies in several independent cohorts of patients with UCB, we identified a novel short-3′UTR isoform of *RAC1* frequently expressed in UCBs, and it was positively associated with patients with UCB advanced clinical stages and/or poor survival. It appears, therefore, that the examination of *RAC1* short-3′UTR isoform might be used as an additional tool to predict those patients with UCB with increased risk of tumor aggressiveness and/or worse prognosis.

In our study, a series of *in vitro* and *in vivo* assays were then employed to investigate the biological functions of *RAC1* short-3′UTR isoform in regulating UCBs' malignant phenotype. Our results clearly showed that enforced expression of *RAC1* short-3′UTR isoform in UCB cells substantially promoted their oncogenic and metastatic capacities either *in vitro* or *in vivo*. It is known the *RAC1* gene is an oncogene that plays important roles in the malignant nature of many types of human cancer (33, 34). However, the underlying mechanisms of *RAC1* activation in various types of cancer tend to be varied and complex (35). In our study, we further found that ectopic overexpression of the *RAC1* short-3′UTR isoform in UCB cells dramatically increased protein expression of RAC1 by escaping from miRNA targeted repression and thus, largely up-regulating certain key targets, AKT and β-catenin-MMP9 pathways, which can potently stimulate cancer cell proliferation and invasion (36, 37). These findings suggest that 3′UTR shortening of *RAC1* in UCB is a critical mechanism to upregulate RAC1 expression and consequently promote UCBs tumorigenesis and/or progression.

One of the most interesting questions was then raised up, i.e., what is the potential mechanisms governing the 3′UTR shortening of *RAC1* in UCB? It has been reported that genetic deletion or aberrations may directly result in 3′UTR shortening (4). Because no disease-causative mutations have been clarified in *RAC1* gene from UCBs in the TCGA database, we excluded out the possibility of *cis*-regulation in *RAC1* 3′UTR shortening in UCB. Next, by screening the expression of 6 well-known CPA factors in our UCB cohorts, we identified that overexpression of CSTF2 in UCBs positively correlated with high usages of the short *RAC1* 3′UTR isoform. Moreover, knockdown of CSTF2 in UCB cells, but not other CPA factors, largely decreased the ratio of short to long *RAC1* 3′UTR. These results together provide straightforward evidence that CSTF2 controls the 3′UTR shortening of *RAC1* in UCB.

In the next parts of our study, we therefore further investigated the precise mechanisms by which CSTF2 targets *RAC1* 3′UTR to promote the usage of pPAS in UCB cells. Our data demonstrated that (1) two GUKKU motifs, locating in the 30–50 nt region downstream to the noncanonical pPAS of *RAC1*, are critical for CSTF2 recognition; (2) high CSTF2 occupancy governs pPAS selection by mediating a slow RNAPII transcription elongation kinetics at the *RAC1* gene, but not at the other cellular genes, such as *GAPDH*, *B2M*, *CALM2*, and *HPRT1*; and moreover, (3) CSTF2 attenuates the specific recruitment of SEC factors, AFF1 and AFF4, to the *RAC1* pPAS region and phosphorylation of RNAPII Serine-2, resulting in slow transcription elongation. These data, taken together, provided first line of evidences that in human UCB, a slower RNAPII elongation rate medicated by CSTF2 governs pPAS usage in *RAC1* 3′UTR.

Recently, some APA factors, such as CFIm25 (12) and PABPN1 (38), have been implicated in tumorigenicity. CFIm25 was identified in governing APA and links APA to glioblastoma tumor suppression (12). Through bioinformatic APA profiling and analysis, the expression of PABPN1 was found significantly correlated with the dPAS usage in many types of human cancer (38). These

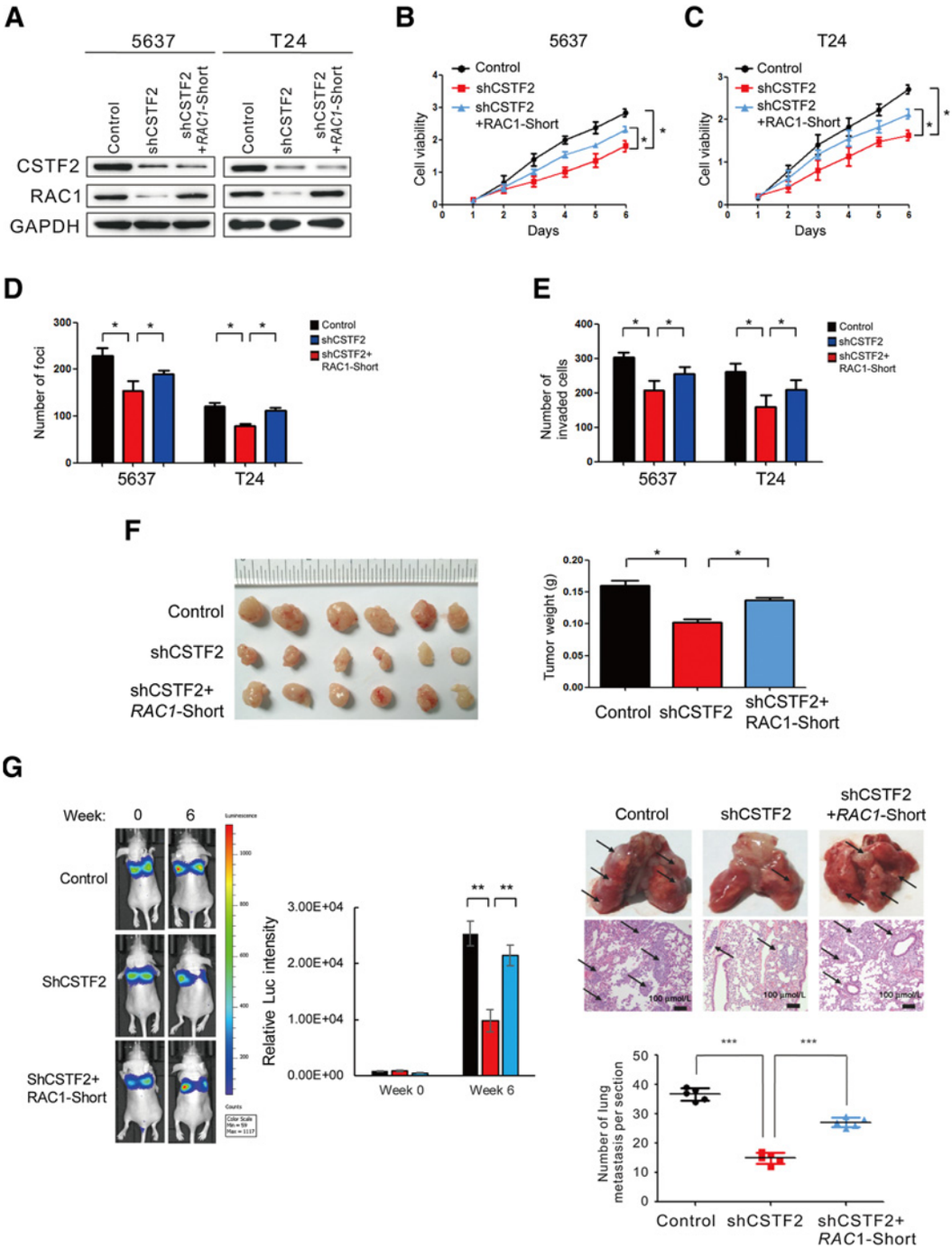

Figure 5.

CSTF2 regulates the oncogenicity and invasiveness of the shorter *RAC1* isoform in UCB. **A,** Protein levels of CSTF2 and RAC1 in UCB 5637 and T24 cells after indicated treatment examined by Western blot. GAPDH expression was used as a loading control. **B–E,** Knockdown of CSTF2 in both 5637 and T24 cells significantly inhibited cell growth (**B** and **C**), colony formation (**D**), and invasion (**E**), respectively, and such could be largely prevented by ectopic overexpression of short-3′UTR *RAC1* isoform in CSTF2-silenced UCB cells (**B–E**). All graphs represent mean ± SD obtained from three independent experiments. *, $P < 0.05$; **, $P < 0.01$, Student *t* test. **F,** Xenograft tumor formation in Balb/c nude mice injected with CSTF2-depleted T24 cells was inhibited as compared with that of control cells. Decreased tumor formation was rescued by overexpression of the short-3′UTR *RAC1* isoform in CSTF2-silenced cells. Left, images of the xenograft tumors formed in mice. Right, quantification of xenograft tumor weights. *, $P < 0.05$; **, $P < 0.01$, Student *t* test. **G,** T24 cells infected with the indicated lentiviruses were injected into the vein of Balb/c nude mice, followed by noninvasive bioluminescence imaging for 6 weeks. Representative bioluminescent imaging (left), representative images of lungs (top right), metastatic nodules (arrows) are shown. The lung metastasis in mice injected with CSTF2-silenced T24 cells was significantly suppressed compared with that of control cells, whereas overexpression of the short-3′UTR *RAC1* isoform abrogated the effect of CSTF2 depletion on lung metastasis. Middle, hematoxylin and eosin staining of lung metastatic tumors (original magnification, ×100; scale bar, 100 μm). Bottom, number of metastatic nodules formed in the lung of mice is summarized for each tested group (5 mice per group). *, $P < 0.05$; **, $P < 0.01$, Student *t* test.

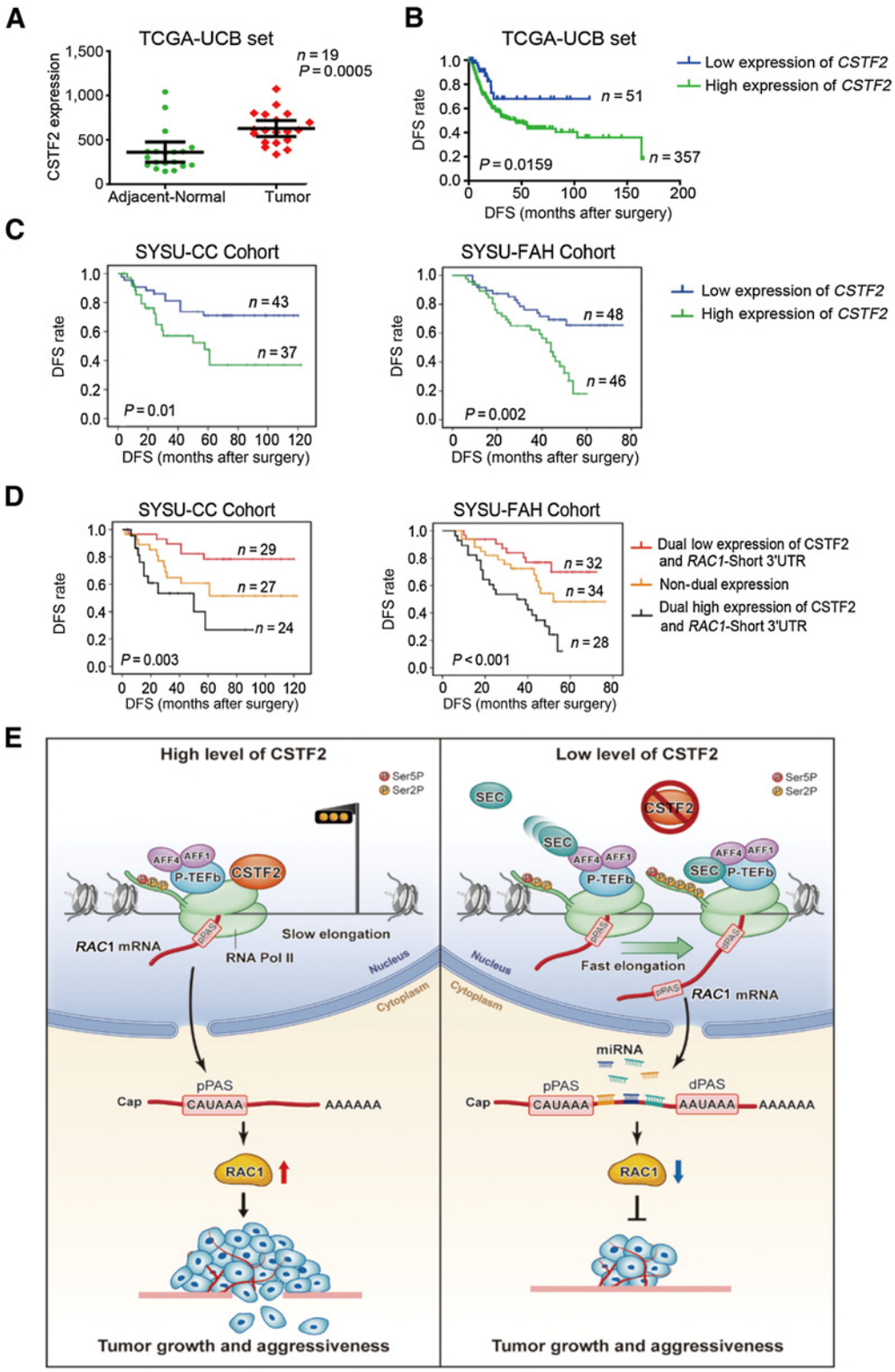

Figure 6.

Dual high expression of CSTF2 and *RAC1* with short-3′UTR predicts worse patient prognosis in UCBs. **A,** A scatter plot shows relative mRNA expression levels of *CSTF2* in UCB tissues and matched adjacent nontumor tissues derived from TCGA. **B,** Kaplan–Meier analysis on DFS in patients with UCB with low versus high expression of *CSTF2* mRNA from TCGA ($P < 0.001$, log-rank analysis). **C,** Kaplan–Meier analysis of DFS in patients with UCB with low versus high expression of CSTF2 protein from the SYSU-CC (left) and SYSU-FAH (right) cohorts. **D,** Patients with UCB with dual high expression of CSTF2 and *RAC1* with short-3′UTR have significantly lower DFS than patients with dual low expression group or patients with high expression of a single factor in the SYSU-CC (left) and SYSU-FAH (right) cohorts. **E,** Schematic diagram depicting a proposed model for the role and a major mechanism of *RAC1* 3′UTR shortening induced by CSTF2 in UCB pathogenesis.

studies, together, give a hint that the dysregulated expression of certain APA factors may be the key players for the aberrant APA events and core regulators in tumorigenesis. So far, the function of CSTF2 has been previously well-characterized in mRNA 3′-end formation (39). However, the pathologic functions of CSTF2 in human disease, especially in cancers, have not been clearly elucidated. To our knowledge, there is only one report that documented that CSTF2 is overexpressed in lung cancers, and it is correlated closely with patients' poor prognosis (40). Thus, in the last part of our study, through abundant *in vitro* and *in vivo* studies, we confirmed that CSTF2 contributes to the oncogenic functions of *RAC1* short-3′UTR isoform in UCB, and dual high expression of CSTF2 and high usage of *RAC1* short-3′UTR isoform predict the poorest DFS of a patient with UCB. Therefore, as a result of our collective present data, herein we propose a model to reveal the molecular mechanism of *RAC1* 3′UTR shortening through CSTF2-mediated APA regulation in promoting UCB pathogenesis, and it is illustrated in Fig. 6E.

In summary, our report describes, for the first time, that 3′UTR shortening of *RAC1* is a frequent oncogenic event in UCBs, and it is important in the tumorigenesis and acquisition of an aggressive/poor prognostic phenotype of the disease. In addition, functional and mechanistic studies as provided in this study demonstrate that CSTF2 exerts critical roles in activation of *RAC1* by promoting 3′UTR shortening of *RAC1* mRNAs through two transcription elongation factors, AFF1 and AFF4, in UCB pathogenesis. Importantly, our finding might offer two novel therapeutic targets, CSTF2 and short-3′UTR isoform of *RAC1*, to broaden the treatment options for human UCB.

Disclosure of Potential Conflicts of Interest

No potential conflicts of interest were disclosed.

Authors' Contributions

Conception and design: X. Chen, S. Wu, F.-J. Zhou, D. Xie
Development of methodology: S. Wu, G.-J. Yuan
Acquisition of data (provided animals, acquired and managed patients, provided facilities, etc.): J.-X. Zhang, Y. Feng, L.-J. Jiang, F.-J. Zhou
Analysis and interpretation of data (e.g., statistical analysis, biostatistics, computational analysis): J.-X. Zhang, J.-H. Luo, S. Wu, G.-J. Yuan, N.-F. Ma, J. Lu, H.-L. Liu, T.-B. Kang, D. Xie
Writing, review, and/or revision of the manuscript: X. Chen, S. Wu, F.-J. Zhou, D. Xie
Administrative, technical, or material support (i.e., reporting or organizing data, constructing databases): X. Chen, M.-Y. Cai, R.-X. Chen, J.-W. Chen, X.-H. Jin, X.-Y. Guan, F.-J. Zhou
Study supervision: J.-W. Chen, T.-B. Kang, F.-J. Zhou, D. Xie

Acknowledgments

We are grateful to the TCGA research network for providing the data analyzed in this article. This work was supported by grants from the National Key R&D Program of China (No. 2017YFC1309001 and No. 2016YFC1302305; D. Xie) and the National Natural Science Foundation of China [Nos. 81602233 (X. Chen), 81672530 (F.J. Zhou), and 81730072 (D. Xie)].

The costs of publication of this article were defrayed in part by the payment of page charges. This article must therefore be hereby marked *advertisement* in accordance with 18 U.S.C. Section 1734 solely to indicate this fact.

Received March 28, 2018; revised July 6, 2018; accepted August 15, 2018; published first August 24, 2018.

References

1. Jemal A, Bray F, Center MM, Ferlay J, Ward E, Forman D. Global cancer statistics. CA Cancer J Clin 2011;61:69–90.
2. Sternberg CN, Bellmunt J, Sonpavde G, Siefker-Radtke AO, Stadler WM, Bajorin DF, et al. ICUD-EAU International Consultation on Bladder Cancer 2012: chemotherapy for urothelial carcinoma-neoadjuvant and adjuvant settings. Eur Urol 2013;63:58–66.
3. Mayr C, Bartel DP. Widespread shortening of 3'UTRs by alternative cleavage and polyadenylation activates oncogenes in cancer cells. Cell 2009; 138:673–84.
4. Kataoka K, Shiraishi Y, Takeda Y, Sakata S, Matsumoto M, Nagano S, et al. Aberrant PD-L1 expression through 3'-UTR disruption in multiple cancers. Nature 2016;534:402–6.
5. Xia Z, Donehower LA, Cooper TA, Neilson JR, Wheeler DA, Wagner EJ, et al. Dynamic analyses of alternative polyadenylation from RNA-seq reveal a 3'-UTR landscape across seven tumour types. Nat Commun 2014;5:5274.
6. Di Giammartino DC, Nishida K, Manley JL. Mechanisms and consequences of alternative polyadenylation. Mol Cell 2011;43:853–66.
7. Farh KK, Grimson A, Jan C, Lewis BP, Johnston WK, Lim LP, et al. The widespread impact of mammalian MicroRNAs on mRNA repression and evolution. Science 2005;310:1817–21.
8. Lembo A, Di Cunto F, Provero P. Shortening of 3'UTRs correlates with poor prognosis in breast and lung cancer. PLoS One 2012;7:e31129.
9. Morris AR, Bos A, Diosdado B, Rooijers K, Elkon R, Bolijn AS, et al. Alternative cleavage and polyadenylation during colorectal cancer development. Clin Cancer Res 2012;18:5256–66.
10. Wittekind C. [2010 TNM system: on the 7th edition of TNM classification of malignant tumors]. Pathologe 2010;31:331–2.
11. Trapnell C, Pachter L, Salzberg SL. TopHat: discovering splice junctions with RNA-Seq. Bioinformatics 2009;25:1105–11.
12. Masamha CP, Xia Z, Yang J, Albrecht TR, Li M, Shyu AB, et al. CFIm25 links alternative polyadenylation to glioblastoma tumour suppression. Nature 2014;510:412–6.
13. Li XD, Zhang JX, Jiang LJ, Wang FW, Liu LL, Liao YJ, et al. Overexpression of maelstrom promotes bladder urothelial carcinoma cell aggressiveness by epigenetically downregulating MTSS1 through DNMT3B. Oncogene 2016; 35:6281–92.
14. He LR, Liu MZ, Li BK, Rao HL, Deng HX, Guan XY, et al. Overexpression of AIB1 predicts resistance to chemoradiotherapy and poor prognosis in patients with primary esophageal squamous cell carcinoma. Cancer Sci 2009;100:1591–6.
15. Yu C, Liu Z, Chen Q, Li Y, Jiang L, Zhang Z, et al. Nkx2.8 inhibits epithelial-mesenchymal transition in bladder urothelial carcinoma via transcriptional repression of Twist1. Cancer Res 2018;78:1241–52.
16. Veloso A, Kirkconnell KS, Magnuson B, Biewen B, Paulsen MT, Wilson TE, et al. Rate of elongation by RNA polymerase II is associated with specific gene features and epigenetic modifications. Genome Res 2014;24: 896–905.
17. Saponaro M, Kantidakis T, Mitter R, Kelly GP, Heron M, Williams H, et al. RECQL5 controls transcript elongation and suppresses genome instability associated with transcription stress. Cell 2014; 157:1037–49.
18. Camp RL, Dolled-Filhart M, Rimm DL. X-tile: a new bio-informatics tool for biomarker assessment and outcome-based cut-point optimization. Clin Cancer Res 2004;10:7252–9.
19. Polakis PG, Weber RF, Nevins B, Didsbury JR, Evans T, Snyderman R. Identification of the ral and rac1 gene products, low molecular mass GTP-binding proteins from human platelets. J Biol Chem 1989;264: 16383–9.
20. Kinsella BT, Erdman RA, Maltese WA. Carboxyl-terminal isoprenylation of ras-related GTP-binding proteins encoded by rac1, rac2, and ralA. J Biol Chem 1991;266:9786–94.
21. Stacey SN, Sulem P, Jonasdottir A, Masson G, Gudmundsson J, Gudbjartsson DF, et al. A germline variant in the TP53 polyadenylation signal confers cancer susceptibility. Nat Genet 2011;43:1098–103.

22. Yao C, Biesinger J, Wan J, Weng L, Xing Y, Xie X, et al. Transcriptome-wide analyses of CstF64-RNA interactions in global regulation of mRNA alternative polyadenylation. PNAS 2012;109:18773–8.
23. Naganuma T, Nakagawa S, Tanigawa A, Sasaki YF, Goshima N, Hirose T. Alternative 3'-end processing of long noncoding RNA initiates construction of nuclear paraspeckles. EMBO J 2012;31:4020–34.
24. Kim S, Yamamoto J, Chen Y, Aida M, Wada T, Handa H, et al. Evidence that cleavage factor Im is a heterotetrameric protein complex controlling alternative polyadenylation. Genes Cells 2010;15:1003–13.
25. Jenal M, Elkon R, Loayza-Puch F, van Haaften G, Kuhn U, Menzies FM, et al. The poly(A)-binding protein nuclear 1 suppresses alternative cleavage and polyadenylation sites. Cell 2012;149:538–53.
26. Lackford B, Yao C, Charles GM, Weng L, Zheng X, Choi EA, et al. Fip1 regulates mRNA alternative polyadenylation to promote stem cell self-renewal. EMBO J 2014;33:878–89.
27. Takagaki Y, Manley JL. RNA recognition by the human polyadenylation factor CstF. Mol Cell Biol 1997;17:3907–14.
28. Hwang HW, Park CY, Goodarzi H, Fak JJ, Mele A, Moore MJ, et al. PAPERCLIP identifies MicroRNA targets and a role of CstF64/64tau in promoting non-canonical poly(A) site usage. Cell Rep 2016;15:423–35.
29. McCracken S, Fong N, Yankulov K, Ballantyne S, Pan G, Greenblatt J, et al. The C-terminal domain of RNA polymerase II couples mRNA processing to transcription. Nature 1997;385:357–61.
30. Mason PB, Struhl K. Distinction and relationship between elongation rate and processivity of RNA polymerase II in vivo. Mol Cell 2005;17:831–40.
31. Zhou Q, Li T, Price DH. RNA polymerase II elongation control. Annu Rev Biochem 2012;81:119–43.
32. Luo Z, Lin C, Guest E, Garrett AS, Mohaghegh N, Swanson S, et al. The super elongation complex family of RNA polymerase II elongation factors: gene target specificity and transcriptional output. Mol Cell Biol 2012;32:2608–17.
33. Marei H, Malliri A. Rac1 in human diseases: The therapeutic potential of targeting Rac1 signaling regulatory mechanisms. Small GTPases 2017;8:139–63.
34. Volanis D, Zaravinos A, Kadiyska T, Delakas D, Zoumpourlis V, Spandidos DA. Expression profile of Rho kinases in urinary bladder cancer. J BUON 2011;16:511–21.
35. Kazanietz MG, Caloca MJ. The Rac GTPase in cancer: from old concepts to new paradigms. Cancer Res 2017;77:5445–51.
36. Liu L, Zhang H, Shi L, Zhang W, Yuan J, Chen X, et al. Inhibition of Rac1 activity induces G1/S phase arrest through the GSK3/cyclin D1 pathway in human cancer cells. Oncol Rep 2014;32:1395–400.
37. Zhang J, Wu N, Gao N, Yan W, Sheng Z, Fan D, et al. Small G Rac1 is involved in replication cycle of dengue serotype 2 virus in EAhy926 cells via the regulation of actin cytoskeleton. Sci China Life Sci 2016;59:487–94.
38. Xiang Y, Ye Y, Lou Y, Yang Y, Cai C, Zhang Z, et al. Comprehensive characterization of alternative polyadenylation in human cancer. J Natl Cancer Inst 2018;110:379–89.
39. MacDonald CC, Wilusz J, Shenk T. The 64-kilodalton subunit of the CstF polyadenylation factor binds to pre-mRNAs downstream of the cleavage site and influences cleavage site location. Mol Cell Biol 1994;14:6647–54.
40. Aragaki M, Takahashi K, Akiyama H, Tsuchiya E, Kondo S, Nakamura Y, et al. Characterization of a cleavage stimulation factor, 3' pre-RNA, subunit 2, 64 kDa (CSTF2) as a therapeutic target for lung cancer. Clin Cancer Res 2011;17:5889–900.